metals

MDPI

Article

Phase Composition, Nanohardness and Young's Modulus in Ti-Fe Alloys after Heat Treatment and High Pressure Torsion

Alena S. Gornakova [1,*], Boris B. Straumal [1,2,3], Andrey A. Mazilkin [1], Natalia S. Afonikova [1], Mikhail I. Karpov [1], Elena A. Novikova [3] and Alexander I. Tyurin [4]

[1] Osipyan Institute of Solid State Physics of the Russian Academy of Sciences, Ac. Osipyan Str. 2, 142432 Chernogolovka, Russia; straumal@issp.ac.ru (B.B.S.); mazilkin@issp.ac.ru (A.A.M.); natasha@issp.ac.ru (N.S.A.); karpov@issp.ac.ru (M.I.K.)

[2] Chernogolovka Scientific Center of the Russian Academy of Sciences, Lesnaja Str. 9, 142432 Chernogolovka, Russia

[3] Department of Physical Chemistry, National University of Science and Technology MISiS, Leninskiy Ave. 4, 119049 Moscow, Russia; e.a.novikova55@mail.ru

[4] G.R. Derzhavin Research Institute "Nanotechnologies and Nanomaterials" TSU, Internazionalnaja Str. 30, 392000 Tambov, Russia; tyurin@tsu.tmb.ru

* Correspondence: alenahas@issp.ac.ru; Tel.: +7-903-239-5060

Abstract: Four titanium-iron binary alloys were studied. They were preliminarily annealed in the (α + β) and (α + TiFe) regions of the Ti-Fe phase diagram. The changes in the phase composition, nanohardness, and Young's modulus of the annealed alloys before and after high pressure torsion (HPT) were investigated. Alloys with high iron content after HPT contain a large fraction of the ω phase. The nanohardness of the material in the middle of the radius of the HPT samples varies in the same range of values between 4.4 and 5.8 GPa, regardless of the preliminary annealing. Young's modulus is a parameter sensitive to structural and phase changes in the material. After HPT, it increases by a factor of 1.5 after preliminary annealing in the (α + β) region in comparison with that in (α + TiFe) region.

Keywords: titanium alloys; high-pressure torsion; Young's modulus; pre-annealing; nanoindentation

Citation: Gornakova, A.S.; Straumal, B.B.; Mazilkin, A.A.; Afonikova, N.S.; Karpov, M.I.; Novikova, E.A.; Tyurin, A.I. Phase Composition, Nanohardness and Young's Modulus in Ti-Fe Alloys after Heat Treatment and High Pressure Torsion. *Metals* **2021**, *11*, 1657. https://doi.org/10.3390/met11101657

Academic Editor: Fantao Kong

Received: 29 September 2021
Accepted: 15 October 2021
Published: 19 October 2021

1. Introduction

Titanium alloys are quite attractive for various applications because of their high specific strength, good corrosion resistance and high biocompatibility [1]. Therefore, the interest in titanium and its alloys increases over the years [2–6]. The alloying, as well as various thermal and mechanical treatments of titanium alloys permit the targeted control of their structure and properties. Unlike many of the broadly used alloys (like Cu-, Al-, Mo-, W- or Ta-based ones etc.), titanium has different allotropic modifications at different temperatures and pressures. From this point of view, it is similar to iron. Therefore, it gives the opportunity to develop various thermal and mechanical treatments technologies for the titanium-based alloys. In particular, titanium has also a high pressure ω-phase (together with low-temperature α and high-temperature β phases). The ω-phase can be observed after pressure release. It is present as metastable one at ambient temperature and disappears only after a heating up to several hundred degrees centigrade [2,3,7–12]. In some Ti-alloys the metastable ω-phase appears even after a certain heat treatment, without application of high pressure [13–16].

The important input to the development of new ways to improving the properties of Ti-based alloys can be done using severe plastic deformation (SPD) [2–4,17–21]. In combination with conventional heat treatment, SPD expands the capabilities of titanium alloys and their application area [17]. In particular, SPD can initiate the various phase transitions [22] and always leads to strong grain refinement [23]. Among the SPD-driven phase transformations are decomposition [24–28] of the formation of the supersaturated

solid solution [29–31], nanocrystallization [32–34], dissolution of particles of a second solid phase [35–40], amorphization [41–46], etc. The SPD (together with proper heat treatment) allows controlling phase transformations and, therefore, tailoring the properties of a material [17,47–50]. It is known that the phase composition, microstructure and mechanical properties of alloys after severe plastic deformation are affected by the applied pressure [18], the temperature during deformation [19], impurities [3,20], strain value [3,21,26], strain rate [51], as well as the orientation of the grains in the starting material [21].

In many cases, various SPD-driven phase transformations proceed simultaneously and, therefore, can compete with each other [27,50]. Several SPD-driven phase transitions in the literature include mass-transfer and are, therefore, diffusive [23–51]. However, the SPD can induce also displacive (or martensitic) phase transitions [50–56]. Using the microstructure peculiarities of Ti-alloys induced by SPD, one can reach the excellent mechanical properties [48,55,57] like the extraordinarily combination of high ductility and strength [58,59]. Thus, SPD allows for the improving of the structure and properties of Ti-based alloys. Therefore, the purpose of this work is to study the binary titanium-iron alloys with different compositions annealed just below and above the temperature of eutectoid transformation and subsequently subjected to the high pressure torsion (HPT), and to analyze the resulting changes of nanohardness and Young's modulus of these alloys.

2. Materials and Methods

Four binary titanium-iron alloys with 1.98 ± 0.12 wt.% Fe, 2.04 ± 0.07 wt.% Fe, 2.36 ± 0.03 wt.% Fe and 3.93 ± 0.21 wt.% Fe were studied. The alloys were manufactured of pure titanium (99.98%, TI-1 grade) and iron (99.97%) by the levitation method in an atmosphere of pure argon. In this method the molten metal levitates in a so-called cold crucible, consisting of a circular set of vertically standing, water-cooled copper tubes. Around the cold crucible is a water-cooled copper induction coil, which excites a powerful magnetic field with a supersonic frequency in the cold crucible. Foucault eddy currents are induced in the molten metal, which cause intense heating of the metal, up to its melting point. At the same time, eddy currents create a counter magnetic field around the melt, which interacts with the primary field and generates Lorentz forces, which allow a liquid metal bath to float in a vacuum or inert atmosphere without touching the walls of a cold crucible.

The discs with a thickness of 0.7 mm and diameter of 10 mm were cut from the obtained cylindrical ingots. Then each sample was sealed in a quartz ampoule and annealed in vacuum at a residual pressure of 4×10^{-4} Pa. After annealing, the samples were quenched in water together with an ampoule. Annealings were carried out in two regions of the titanium-iron phase diagram (above and below the eutectoid transformation), namely in α + β area at 615 °C (144 and 270 h) and in α + TiFe area at 470 °C (463 and 750 h). HPT was performed using a custom built computer-controlled device manufactured by W. Klement GmbH, Lang, Austria. The obtained samples were subjected to HPT at room temperature at 7 GPa, deformation rate of 1 rpm and 5 revolutions of the plunger. After the HPT, the thickness of the samples was 0.35 mm.

Measurements of the nanohardness were carried out on the TI-950 Hysitron Triboindenter device equipped with a Berkovich indenter (Brucker, Madison, WI, USA). The measurements were carried out in the center (R_0), in the middle of the radius ($R_{1/2}$) and near the edge (R_1) of the samples, the loading rate was constant and equal to dP/dt = 40 mN/s. The maximal load was P_{max} = 200 mN. Before the measurements, the surface of the samples was polished on a diamond paste with a grain size of 1 microns. The numerical values of the nanohardness (H) and Young's modulus (E) of the studied samples were determined using the Oliver-Farr method based on characteristic P-h diagrams [60–62]. Nanohardness measurements were carried out at room temperature and a constant value of the maximum load applied to the P_{max} indenter (P_{max} = 200 mN), the studied values of H and E were obtained by averaging the results obtained from 12 independent experiments.

For the structural-phase analysis of the samples, the X-ray (XRD) patterns were measured using a Siemens D-500 X-ray diffractometer (Berlin, Germany) in Cu-K_1 radiation. The phase analysis and calculation of the lattice parameters were carried out using the PowderCell for Windows Version 2.4.08.03.2000 program (Werner Kraus & Gert Nolze, BAM, Berlin, Germany). To determine the chemical composition of the samples, a high-resolution scanning electron microscope (SEM) Supra 50VP (Carl Zeiss, Oberkochen, Germany) with the INCA Energy + microanalysis system was used, equipped with an Oxford Instruments (Abingdon, UK) energy dispersion microanalysis prefix. Transmission electron microscopy (TEM) and high resolution TEM (HRTEM) observations have been made by using an aberration corrected TITAN 80–300 transmission electron microscope (FEI, Hillsboro, OR, USA). The cross section TEM and HRTEM specimens were cut from HPT discs at a 3 mm distance from the disc center. They were further thinned in a FEI Strata 400S dual beam facility (FEI, Hillsboro, OR, USA).

3. Results

Figure 1 shows XRD patterns for the Ti–2.36 wt.% Fe (Figure 1a), Ti–3.93 wt.% Fe (Figure 1b), Ti–1.98 wt.% Fe (Figure 1c) and Ti–2.04 wt.% Fe (Figure 1d) alloys annealed at 470 °C (Figure 1a,b) and 615 °C (Figure 1c,d). The bottom curves (red) are for the annealed samples before HPT, the top curves (black) are for the annealed samples after HPT. The peaks in XRD patterns before HPT are narrow. It is due to the high crystallinity of the samples and large grain size in the samples after annealing. The peaks in XRD patterns after HPT are broad due to the grain refinement driven by HPT. The samples annealed at 470 °C (Figure 1a,b, red curves), i.e., below the temperature of eutectoid decomposition of β-phase contain the mixture of α-phase and intermetallic compound TiFe. After HPT (Figure 1a,b, black curves) the ω-phase appears in addition to the α-phase and TiFe. The samples annealed at 615 °C (Figure 1c,d, red curves), i.e., above the temperature of eutectoid decomposition of β-phase contain the mixture of α-phase and β-phases. After HPT (Figure 1c,d, black curves) the ω-phase appears, and the α-phase almost disappears.

In Figure 1 some peaks are marked as α/β/ω. After exposure to HPT, the peaks in the XRD patterns become wide and "blurred". As a result, one, two or even three closely lying XRD peaks corresponding to different phases can fall under such a "blurred" peak. The phase analysis and calculation of the lattice parameters were carried out using the PowderCell for Windows Version 2.4.08.03.2000 program (Werner Kraus & Gert Nolze, BAM Berlin, Germany). The program distinguishes all phases and closely lying lines of different phases. The scale of the drawings does not allow us to make more inscriptions and preserve the readability of the text, therefore we used such a system for describing the peaks.

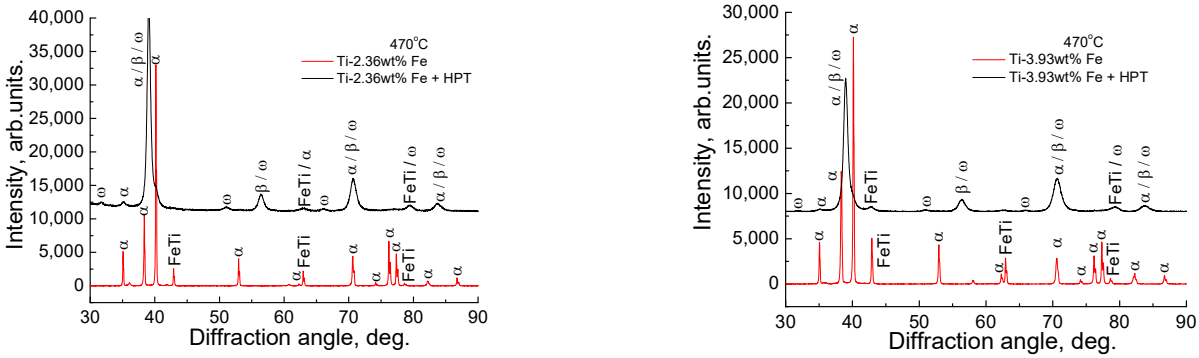

(**a**) (**b**)

Figure 1. *Cont.*

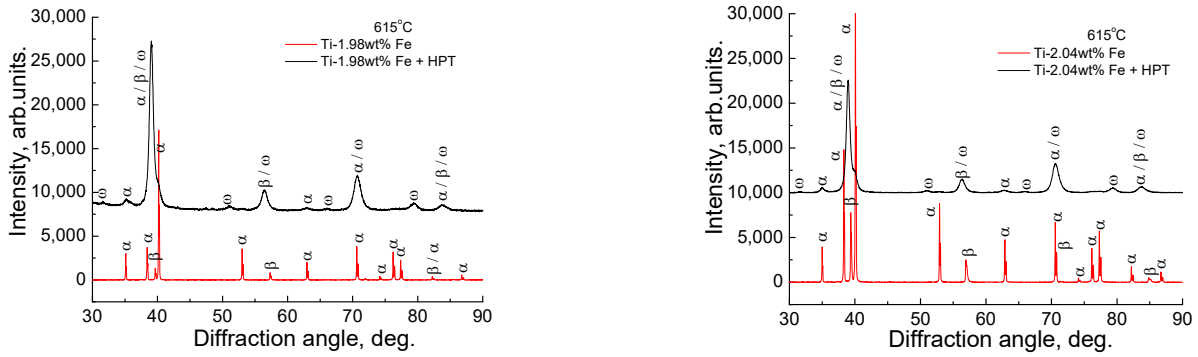

(**c**) (**d**)

Figure 1. XRD patterns for the Ti–2.36 wt.% Fe (**a**), Ti–3.93 wt.% Fe (**b**), Ti–1.98 wt.% Fe (**c**) and Ti–2.04 wt.% Fe; and (**d**) alloys annealed at 470 °C (**a**,**b**) and 615 °C (**c**,**d**). The bottom curves (red) are for the annealed samples before HPT, the top curves (black) are for the annealed samples after HPT.

The results of XRD studies of samples before and after HPT are given in Table 1. In all annealed samples, the main phase is α. The average grain size in α and β phases varies from 125 to 144 nm. It has been was calculated from X-ray structural data using the shape of XRD peaks. After HPT the average grain size is 34 ÷ 38 nm in α-phase, 32 ÷ 47 nm in β-phase and 18 ÷ 25 nm in ω-phase. Data on the grain size in different phases before HPT (average 133.6 ± 2.8 nm) and after HPT (average 32.4 ± 2.9 nm) is shown in Figure 2. The main phase after HPT becomes the ω-phase and its fraction increases with increasing iron concentration in the alloy (Table 2). The lattice parameters after annealing and after HPT for the α-phase almost do not change. It can be seen from the tables that the fraction of the β-phase after the HPT decreases, the lattice parameters increase by 0.004 nm, i.e., in the β phase after the HPT, the concentration of iron increases.

Table 1. Lattice parameters, phases and their volume fraction in alloys after heat treatment.

Iron Content, wt.% Fe	Phase Diagram Area	αTi		βTi		TiFe	
		V, %	*a*, *c*, nm	V, %	*a*, nm	V, %	*c*, *a*, nm
1.98 ± 0.12	α + β	95	0.2950, 0.4686	5	0.3216	-	-
2.04 ± 0.07	α + β	85	0.2948, 0.4682	15	0.3226	-	-
2.36 ± 0.03	α + TiFe	97	0.2950, 0.4687	-	-	3	0.2978
3.93 ± 0.21	α + TiFe	92	0.2950, 0.4688	-	-	8	0.2976
Ti [63]	-	-	0.2955, 0.4694		-		

Table 2. Lattice parameters, phases and their volume fraction in alloys after heat treatment and HPT.

Iron Content, wt.% Fe	Phase Diagram Area	αTi		βTi		ωTi		TiFe	
		V, %	*a*, *c*, nm	V, %	*a*, nm	V, %	*c*, *a*, nm	V, %	*a*, nm
1.98 ± 0.12	α + β	10	0.2952, 0.4693	11	0.3256	79	0.4626, 0.2814	-	-
2.04 ± 0.07	α + β	12	0.2950, 0.4684	1	0.3252	87	0.4630, 0.2812	-	-
2.36 ± 0.03	α + TiFe	8	0.2950, 0.4690	16	0.3255	76	0.4626, 0.2814	-	-
3.93 ± 0.21	α + TiFe	7.5	0.2950, 0.4688	-	-	92	0.4627, 0.2812	0.5	0.2980
Ti [63]	–	-	0.2959, 0.4690	-	-	-	-	-	-

Figure 3 shows the TEM micrographs of the Ti–3.93 wt.% Fe alloy annealed at T = 615 °C, 270 h, quenched and subjected to HPT at 7 GPa, 1 rpm, 5 rot. The bright field image is shown in the left-hand side of the figure, the dark field image is on the right. The grain size is about 50 nm and corresponds with the XRD data. The selected

area electron diffraction (SAED) pattern is shown as inset. It contains the rings of α- and ω-phases.

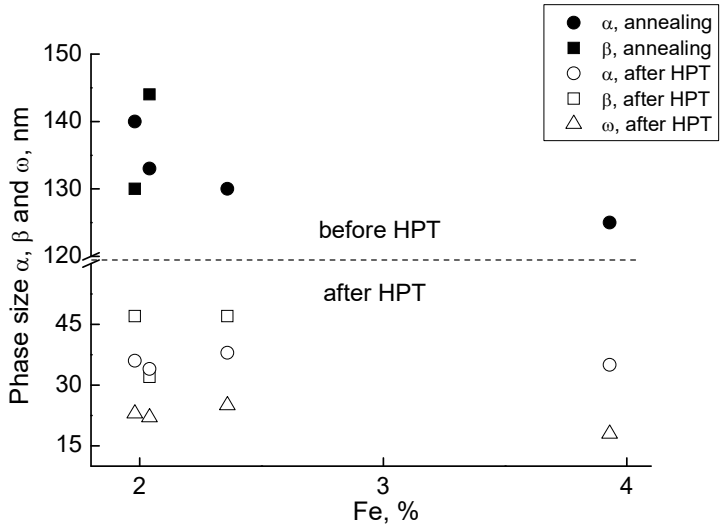

Figure 2. Mean grain size for the α-, β- and ω-phases in the annealed samples before and after HPT.

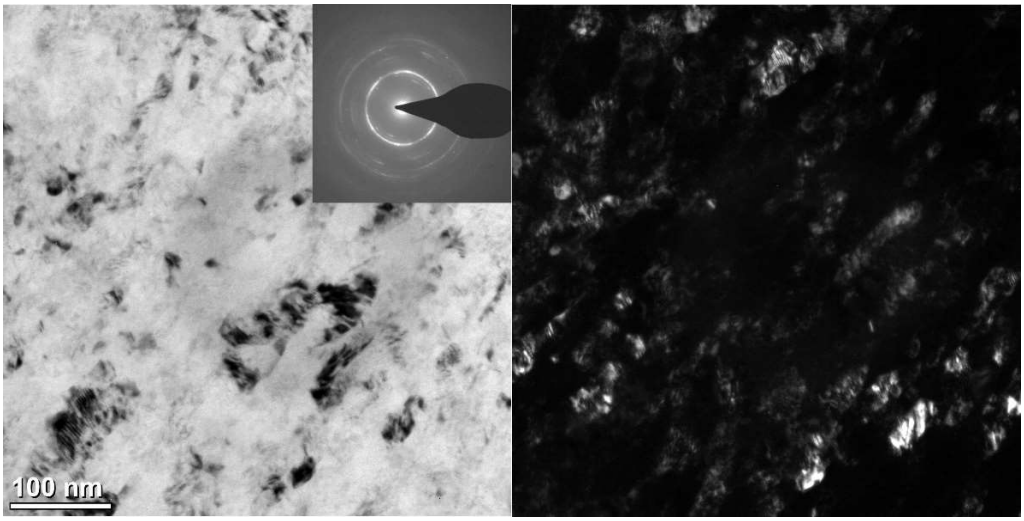

Figure 3. TEM micrographs of the Ti–3.93 wt.% Fe alloy annealed at T = 615 °C, 270 h, quenched and subjected to HPT at 7 GPa, 1 rpm, 5 rot. On the left is a bright field image; on the right is a dark field image of the same area. The selected area electron diffraction (SAED) pattern is shown as inset.

In Figure 4 the dependences are shown between load P applied to the Berkovich indenter and the indentation depth h for the alloys (1) Ti–1.98 wt.% Fe annealed at 470 °C, (2) Ti–2.04 wt.% Fe annealed at 470 °C, (3) Ti–2.36 wt.% Fe annealed at 615 °C, (4) Ti–3.93 wt.% Fe annealed at 615 °C. After preliminary annealing, the samples were subjected to HPT (7 GPa, 1 rpm, 5 rot). The $P(h)$ dependences were measured: (a) in the sample center R_0; (b) in the middle of the radius $R_{1/2;}$ and (c) at the sample edge R_1. The slope of these curves is proportional to the Young's modulus E. It is important that the slope of $P(h)$ curves is very different for different studied samples.

Consider now the dependences of the nanohardness H (Figure 5a,c) and Young's modulus E (Figure 5b,d) on the location of the measurements, namely the center, the middle of the radius and the edge of the samples. In the first case (Figure 5a,b), when the annealing temperature and duration are the same for two alloys, and the iron concentration differs by 1.57 wt.% (~60%), as a result, H is higher by 1.3 GPa (~23%), and E is higher by

46 GPa (~43%) for the Ti–3.93 wt.% Fe alloy in comparison with that with 1.57 wt,% Fe. These values are measured in the middle of the radius of the samples. The differences in the H and E values in the center and at the edges of the samples are higher. In the second case (Figure 5b,d), when the temperature and concentration of iron is the same for the two alloys, and the difference in the annealing duration is 126 h (~47%), H is higher by 1.3 GPa (~23%), and E changes by 8 GPa (~5%) for the Ti–1.98 wt.% Fe alloy as a result.

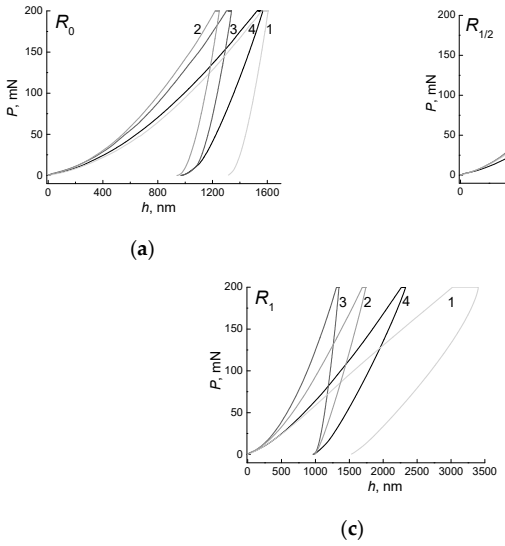

Figure 4. Dependences between load P applied to the Berkovich indenter and the indentation depth h for the alloys (1) Ti–1.98 wt.% Fe annealed at 470 °C, (2) Ti–2.04 wt.% Fe annealed at 470 °C, (3) Ti–2.36 wt.% Fe annealed at 615 °C, (4) Ti–3.93 wt.% Fe annealed at 615 °C. After preliminary annealing, the samples were subjected to HPT (7 GPa, 1 rpm, 5 rot). The $P(h)$ dependences were measured (**a**) in the sample center R_0; (**b**) in the middle of the radius $R_{1/2}$ and (**c**) at the sample edge R_1.

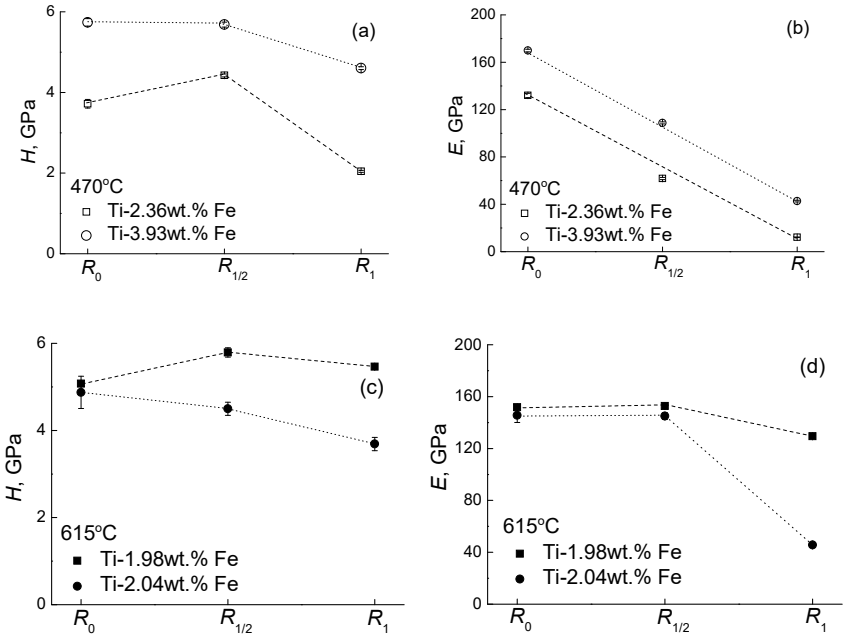

Figure 5. Values of nanohardness and Young's modulus measured after HPT in the center (R_0), in the middle of the radius ($R_{1/2}$) and at the edge (R_1) of the samples for the alloys: (**a**,**b**) Ti–2.36 wt.% Fe and Ti–3.93 wt.% Fe preliminarily annealed at 615°C; (**c**,**d**) Ti–1.98 wt.% Fe and Ti–2.04 wt.% Fe, preliminarily annealed at 470 °C.

4. Discussion

As mentioned above, titanium possesses the high-pressure ω-phase. The ω-phase can be observed after pressure release in HPT. It is present as a metastable one at ambient temperature and disappears only after heating up to several hundred degrees centigrade [2,3,7–12]. In some Ti-alloys the metastable ω-phase appears even after a certain heat treatment, without the application of high pressure [13–16]. The α-Ti phase possesses the space group P63/mmc. α-Ti has two atoms per unit cell at (1/3,2/3,1/2) and (2/3,1/3, 3/2) and a *c/a* ratio of ~1.58. The ω-Ti possesses the space group P6/mmm. It has three atoms per unit cell at (0,0,0), (1/3,2/3,1/2), and (2/3,1/3,1/2) and a *c/a* ratio of ~0.61. Thus, the symmetry of the ω-Ti is high, 24 point-group operations, the same as for the simple hexagonal structure. The specific electronic structure facilitates the formation of ω-Ti. Titanium has the occupied narrow d-band and the broad sp-bands. Under the applied pressure, the sp-bands rise in energy and cause the electrons to be transferred into the d-band [64]. This process is known as s-d transition and governs the structural properties of the transition metals. The elements stabilizing the β-phase in titanium are mostly transition ones (e.g., Nb, Cr, Zr, Fe, Ni, Cu, Co). They are rich on d-electrons. Thus, the alloying of titanium by the β-stabilizers increases the d-electron concentration. Such alloying can, therefore, provide an additional driving force for the αTi to to ωTi transformation. For the $\alpha \rightarrow \omega$ phase transformation, one can consider the alloying of Ti with β-phase stabilizers as an equivalent of pressure. Hennig [65] concluded from ab initio calculations that the alloying with β-stabilizing elements such as V, Mo, Fe or Ta should lead to a decrease in the onset pressure of the $\alpha \rightarrow \omega$ transformation. The combined effect of β-stabilizer alloying and pressure application (2–12 GPa) was experimentally studied using Zr–Nb, Ti–Nb and Ti–V alloys only in few works [66–68]. With increasing concentration of β-stabilizer, the formation pressure of ω-Ti first decreases. Above a certain concentration of a β-stabilizer the formation pressure of ω-Ti rapidly grows.

As a rule, studies conducted on materials after SPD are accompanied by a study of the microstructure, phase composition of samples and measurement of mechanical properties, such as nano- or microhardness [24,25,27,65,66] and elastic modulus [6,69]. One has to underline here the difference between nano and microhardness. When one refers to the "hardness" of a material, one means the property of the material to resist the penetration of a harder material, i.e., the indenter. It is necessary to clearly distinguish between the microhardness and nanohardness of the material. The "nano" prefix reflects the ability of the instruments to measure the displacement of the indenter with a nanometer resolution and operate in the load range from tens to hundreds of nanonewtons to about 10 N. Nanoindentation is realized during tests when the indenter penetration depth h is below 200 nm, microindentation is performed by an indentation force P up to 2 N at $h > 0.2$ μm, and macroindentation is performed by a force P from 2 N to 30 kN. The value of nanohardness can differ significantly from the microhardness for the same material [70–72]. In our work, the nanohardness of the material was measured at P_{max} = 200 mN.

The measured dependences of microhardness along the sample diameter usually have a minimum in the center [3]. Such a minimum in the middle of the sample usually disappears with an increase in the number of revolutions (i.e., with increasing strain). The authors [3] showed that with an increase in the iron concentration from 0 to 1 wt.%, the microhardness of the material increases, and after HPT at 6 GPa it changes in the range from 3.5 to 4.0 GPa, where the main phase in the sample is the ω phase and a little α phase is present. It was shown by Sinha et al. that the hardness of pure titanium increases after HPT with the number of revolutions from the center to the edge in [21]. The authors of reference [21] also concluded that the hardness depends not only on the volume fraction of the α, β or ω phase, but also on the size and distribution of the phases. Edalati et al. showed that carrying out HPT at low temperatures leads to a decrease in the grain size, as well as to a change in the phase ratio [19]. It is shown that the difference of HPT temperature of 200K gives a decrease in the grain size of about a factor of five, and reduces the fraction of the ω phase. In references [62,73], the authors made detailed

measurements of the micro- and nanohardness of large β and α grains in the annealed polycrystal, and showed that the microhardness of β grains in pure titanium increases with increasing annealing duration (from ~1.9 to 2.5 GPa), and microhardness of α-phase decreases from ~2 to 1.8 GPa). Kao [19] suggested that grain boundaries are the main structural component responsible for the strengthening of a material. Chong [73] was able to measure the nanohardness of individual α (3.9 GPa) and β (un-transformed 5.9 GPa and transformed 4.6 GPa) grains in the Ti-1.0 wt.%Fe alloy.

The studied alloys were annealed in two different regions of the phase diagram, namely (α + β) and (α + TiFe). At the studied iron concentrations, the alloys have similar composition and grain size of α, β and TiFe phases. Moreover, after HPT they also have similar values of the phase composition and grain size of for different phases. The spread in nanohardness values after HPT is between 4.4 to 5.8 GPa and is the same for both pre-annealing temperatures. The microhardness of pure titanium (99.4 wt.%) increases from 260 to 400 HV with an increase in the applied HPT pressure [18]. The increase in the number of revolutions also leads to the microhardness increase from 200 to 320 HV [2]. This is the standard spread in the Vickers microhardness for titanium and titanium alloys with a small fraction of the second component [2,3,20,61–63]. The nanohardness values in titanium samples after HPT are from 4 to 6 GPa [69,73,74]. It is about 66% higher than microhardness ones. Thus, our data on nanohardness (Figure 5) do not contradict the published data of other authors. Our alloys with the highest and lowest iron content showed similar hardness values. We can see (Figure 5) that preliminary heat treatment has a significant effect on the mechanical properties of the samples after HPT. The presence of even very small amounts of the intermetallic phase TiFe increases the nanohardness for the samples previously annealed in the (α + TiFe) region. The combination of three phases α, β and ω in the alloy also increases the nanohardness of the material. As can be seen from Figure 5a,b, the multiphase alloy pre-annealed in the temperature region (α + TiFe) has a higher nanohardness value, despite the fact that it contains less iron. The presence of small precipitates of various phases strengthens the material. The values of Young's moduli in this case turned out to be almost equal over the entire radius of the samples.

The literature data on the modulus of elasticity for titanium alloys are more scarce than those for hardness, and their scatter is rather large [69,75–77]. From the results of the experiment shown in Figure 5a,c, it can be seen that two main factors affecting the nanohardness of alloys are the concentration of iron and the phase composition or their combination. A large concentration of iron in the alloy leads to the fact that after HPT the small amounts of the intermetallic compound TiFe remain. These TiFe precipitates, we assume, strengthen the material stronger than a large number of phases in the material. But in this case, the values of Young's modulus fall by almost 1.5–2 times.

If it is required to strengthen the material after exposure to HPT, then it is necessary to select the composition of the material and the area of the phase diagram for preliminary heat treatment. If high values of Young's modulus are required, then pre-annealing in the two-phase region and multiplicity of phases after HPT will raise its values. Two factors have a decisive influence on the micro/nanohardness of the material, namely the presence of intermetallic phase and the precipitates at the grain boundaries.

5. Conclusions

High pressure torsion (HPT) unduces to the phase transitions in the Ti-based alloys. In particular, HPT leads to the formation of a high-pressure ω-Ti phase which remains metastable after pressure release. Phase composition of the samples depends on the phasestemperature of preliminary annealing (above or below the temperature of eutectoid transformation). In turn, the component and phase composition after HPT control the nanohardness *H* and Young's modulus *E*. in such a way that *H* and *E* also depend on the region of the phase diagram in which the preliminary heat treatment is carried out. Preliminary heat treatment in (α + β) region gives high values of Youngs modulus *E*. The increase of the nanohardness *H* of the material requires either the presence of an

intermetallic phase, which can be obtained after annealing in the (α + TiFe) region, or a larger number of different phases.

Author Contributions: Conceptualization, B.B.S. and M.I.K.; methodology, E.A.N.; software, A.I.T.; validation, A.I.T., A.S.G. and A.A.M.; formal analysis, E.A.N.; investigation, A.S.G., A.I.T., N.S.A. and A.A.M.; data curation, A.I.T., N.S.A. and A.A.M.; writing—original draft preparation, A.S.G.; writing—review and editing, B.B.S.; visualization, A.I.T. and A.A.M.; supervision, B.B.S.; project administration, A.S.G.; funding acquisition, B.B.S. All authors have read and agreed to the published version of the manuscript.

Funding: This research was funded by the Russian Ministry of Science and Higher Education (contract No. 075-15-2021-999 grant No. 13.2251.21.0058).

Data Availability Statement: Data is contained within the article.

Acknowledgments: Equipment for metallographic preparation and furnaces for high-temperature annealing of samples were provided by ISSP RAS.

Conflicts of Interest: The authors declare no conflict of interest. The funders had no role in the design of the study; in the collection, analyses, or interpretation of data; in the writing of the manuscript, or in the decision to publish the results.

References

1. Donachie, M.J., Jr. *Titanium: A Technical Guide*, 2nd ed.; ASM International: Materials Park, OH, USA, 2000.
2. Chen, W.; Xu, J.; Liu, D.; Bao, J.; Sabbaghianrad, S.; Shan, D.; Guo, B.; Langdon, T.G. Microstructural evolution and microhardness variations in pure titanium processed by high-pressure torsion. *Adv. Eng. Mater.* **2020**, *22*, 1901462. [CrossRef]
3. Deng, G.; Bhattacharjee, T.; Chong, Y.; Zheng, R.; Bai, Y.; Shibata, A.; Tsuji, N. Characterization of microstructure and mechanical property of pure titanium with different Fe addition processed by severe plastic deformation and subsequent annealing. In *IOP Conference Series: Materials Science and Engineering*; IOP Publishing: Bristol, UK, 2017; Volume 194, p. 012020. [CrossRef]
4. Korneva, A.; Straumal, B.; Kilmametov, A.; Gondek, Ł.; Wierzbicka-Miernik, A.; Litynska-Dobrzynska, L.; Cios, G.; Chulist, R.; Zieba, P. Thermal stability and microhardness of metastable ω-phase in the Ti-3.3 at.% Co alloy subjected to high pressure torsion. *J. Alloys Compod.* **2020**, *834*, 155132. [CrossRef]
5. Mohan, P.; Rajak, D.K.; Pruncu, C.I.; Behera, A.; Amig'o-Borrás, V.; Elshalakany, A.B. Influence of β-phase stability in elemental blended Ti-Mo and Ti-Mo-Zr alloys. *Micron* **2021**, *142*, 102992. [CrossRef] [PubMed]
6. Zhang, W.D.; Liu, Y.; Wu, H.; Song, M.; Zhang, T.Y.; Lan, X.D.; Yao, T.H. Elastic modulus of phases in Ti–Mo alloys. *Mater. Charact.* **2015**, *106*, 302–307. [CrossRef]
7. Errandonea, D.; Meng, Y.; Somayazulu, M.; Häusermann, D. Pressure-induced alpha-to-omega transition in titanium metal: A systematic study of the effects of uniaxial stress. *Phys. B* **2005**, *355*, 116–125. [CrossRef]
8. Trinkle, D.R.; Hennig, R.G.; Srinivasan, S.G.; Hatch, D.M.; Jones, M.D.; Stokes, H.T.; Albers, R.C.; Wilkins, J.W. New mechanism for the alpha to omega martensitic transformation in pure titanium. *Phys. Rev. Lett.* **2003**, *91*, 025701. [CrossRef]
9. Kriegel, M.J.; Kilmametov, A.; Rudolph, M.; Straumal, B.B.; Gornakova, A.S.; Stöcker, H.; Ivanisenko, Y.; Fabrichnaya, O.; Hahn, H.; Rafaja, D. Transformation pathway upon heating of Ti–Fe alloys deformed by high-pressure torsion. *Adv. Eng. Mater.* **2018**, *20*, 1700933. [CrossRef]
10. Kriegel, M.J.; Kilmametov, A.; Klemm, V.; Schimpf, C.; Straumal, B.B.; Gornakova, A.S.; Ivanisenko, Y.; Fabrichnaya, O.; Hahn, H.; Rafaja, D. Thermal stability of athermal ω-Ti(Fe) produced upon quenching of β-Ti(Fe). *Adv. Eng. Mater.* **2019**, *21*, 1800158. [CrossRef]
11. Kriegel, M.J.; Rudolph, M.; Kilmametov, A.; Straumal, B.B.; Ivanisenko, J.; Fabrichnaya, O.; Hahn, H.; Rafaja, D. Formation and thermal stability of ω-Ti(Fe) in α-phase-based Ti(Fe) alloys. *Metals* **2020**, *10*, 402. [CrossRef]
12. Korneva, A.; Straumal, B.B.; Kilmametov, A.R.; Gondek, Ł.; Wierzbicka-Miernik, A.; Lityńska-Dobrzyńska, L.; Chulist, R.; Cios, G.; Zięba, P. The α↔ω phase transformations and thermal stability 2194 of Ti–Co alloy treated by high pressure torsion. *Mater. Charact.* **2021**, *80*, 110937. [CrossRef]
13. Sikka, S.K.; Vohra, Y.K.; Chidambaram, R. Omega-phase in materials. *Prog. Mater. Sci.* **1982**, *27*, 245–310. [CrossRef]
14. Banerjee, S.; Mukhopadhyay, P. *Phase Transformations: Examples from Titanium and Zirconium Alloy*; Elsevier: Amsterdam, The Netherlands, 2010.
15. Hickman, B.S. The formation of omega phase in Ti and Zr alloys: A review. *J. Mater. Sci.* **1969**, *4*, 554–563. [CrossRef]
16. Scientific Group Thermodata Europe (SGTE). Thermodynamic Properties of Inorganic Materials. In *Landolt-Börnstein*; Springer: Berlin/Heidelberg, Germany, 2005; Volume 19, Group IV (Physical Chemistry).
17. Edalati, K.; Matsuda, J.; Arita, M.; Daio, T.; Akiba, E.; Horita, Z. Mechanism of activation of TiFe intermetallics for hydrogen storage by severe plastic deformation using high-pressure torsion. *Appl. Phys. Lett.* **2013**, *103*, 143902. [CrossRef]
18. Edalati, K.; Matsubara, E.; Horita, Z. Processing pure Ti by high-pressure torsion in wide ranges of pressure and strain. *Metall. Mater. Trans. A* **2009**, *40*, 2079–2086. [CrossRef]

19. Edalati, K.; Daio, T.; Arita, M.; Lee, S.; Horita, Z.; Togo, A.; Tanaka, I. High pressure torsion of titanium at cryogenic and room temperatures: Grain size effect on allotropic phase transformation. *Acta Mater.* **2014**, *68*, 207–213. [CrossRef]
20. Wang, C.T.; Fox, A.G.; Langdon, T.G. Microstructural evolution in ultrafinegrained titanium processed by high-pressure torsion under different pressures. *J. Mater. Sci.* **2014**, *49*, 6558–6564. [CrossRef]
21. Sinha, S.; Sahu, V.K.; Beura, V.; Sonkusare, R.; Kalsar, R.; Das, A.K.L.; Basu, J.; Gurao, N.P.; Biswas, K. Initial texture dependence of nanocrystalline omega phase formation during high pressure torsion of commercially pure titanium. *Mater. Sci. Eng. A* **2021**, *802*, 140687. [CrossRef]
22. Straumal, B.; Korneva, A.; Zięba, P. Phase transitions in metallic alloys driven by the high pressure torsion. *Arch. Civ. Mech. Eng.* **2014**, *14*, 242–249. [CrossRef]
23. Valiev, R.Z.; Islamgaliev, R.K.; Alexandrov, I. Bulk nanostructured materials from severe plastic deformation. *Prog. Mater. Sci.* **2000**, *45*, 103–189. [CrossRef]
24. Straumal, B.B.; Baretzky, B.; Mazilkin, A.A.; Phillipp, F.; Kogtenkova, O.A.; Volkov, M.N.; Valiev, R.Z. Formation of nanograined structure and decomposition of supersaturated solid solution during high pressure torsion of Al–Zn and Al–Mg. *Acta Mater.* **2004**, *52*, 4469–4478. [CrossRef]
25. Mazilkin, A.A.; Straumal, B.B.; Rabkin, E.; Baretzky, B.; Enders, S.; Protasova, S.G.; Kogtenkova, O.A.; Valiev, R.Z. Softening of nanostructured Al–Zn and Al–Mg alloys after severe plastic deformation. *Acta Mater.* **2006**, *54*, 3933–3939. [CrossRef]
26. Straumal, B.B.; Protasova, S.G.; Mazilkin, A.A.; Rabkin, E.; Goll, D.; Schütz, G.; Baretzky, B.; Valiev, R. Deformation-driven formation of equilibrium phases in the Cu–Ni alloys. *J. Mater. Sci.* **2012**, *47*, 360–367. [CrossRef]
27. Straumal, B.B.; Kilmametov, A.R.; Kucheev, Y.O.; Kurmanaeva, L.; Ivanisenko, Y.; Baretzky, B.; Korneva, A.; Zięba, P.; Molodov, D.A. Phase transitions during high pressure torsion of Cu–Co alloys. *Mater. Lett.* **2014**, *118*, 111–114. [CrossRef]
28. Straumal, B.; Valiev, R.; Kogtenkova, O.; Zięba, P.; Czeppe, T.; Bielanska, E.; Faryna, M. Thermal evolution and grain boundary phase transformations in severe deformed nanograined Al–Zn alloys. *Acta Mater.* **2008**, *56*, 6123–6131. [CrossRef]
29. Lojkowski, W.; Djahanbakhsh, M.; Burkle, G.; Gierlotka, S.; Zielinski, W.; Fecht, H.J. Nanostructure formation on the surface of railway tracks. *Mater. Sci. Eng. A* **2001**, *303*, 197–208. [CrossRef]
30. Gavriljuk, V.G. Decomposition of cementite in pearlitic steel due to plastic deformation. *Mater. Sci. Eng. A* **2003**, *345*, 81–89. [CrossRef]
31. Sauvage, X.; Wetscher, F.; Pareige, P. Mechanical alloying of Cu and Fe induced by severe plastic deformation of a Cu–Fe composite. *Acta Mater.* **2005**, *53*, 2127–2135. [CrossRef]
32. Glezer, A.M.; Plotnikova, M.R.; Shalimova, A.V.; Dobatkin, S.V. Severe plastic deformation of amorphous alloys: I. Structure and mechanical properties. *Bull. Russ. Acad. Sci. Phys.* **2009**, *73*, 1233–1236. [CrossRef]
33. Abrosimova, G.E.; Aronin, A.S.; Dobatkin, S.V.; Kaloshkin, S.D.; Matveev, D.V.; Rybchenko, O.G.; Tatyanin, E.V.; Zverkova, I.I. The formation of nanocrystalline structure in amorphous Fe-Si-B alloy by severe plastic deformation. *J. Metastab. Nanocryst. Mater.* **2005**, *24*, 69–72. [CrossRef]
34. Henits, P.; Révész, Á.; Zhilyaev, A.P.; Kovács, Z. Severe plastic deformation induced nanocrystallization of melt-spun $Al_{85}Y_8Ni_5Co_2$ amorphous alloy. *J. Alloys Comp.* **2008**, *461*, 195–199. [CrossRef]
35. Cepeda-Jiménez, C.M.; García-Infanta, J.M.; Zhilyaev, A.P.; Ruano, O.A.; Carreño, F. Influence of the thermal treatment on the deformation-induced precipitation of a hypoeutectic Al–7 wt% Si casting alloy deformed by high-pressure torsion. *J. Alloys Comp.* **2011**, *509*, 636–643. [CrossRef]
36. Ivanisenko, Y.; Lojkowski, W.; Valiev, R.Z.; Fecht, H.J. The mechanism of formation of nanostructure and dissolution of cementite in a pearlitic steel during high pressure torsion. *Acta Mater.* **2003**, *51*, 5555–5570. [CrossRef]
37. Straumal, B.B.; Mazilkin, A.A.; Protasova, S.G.; Dobatkin, S.V.; Rodin, A.O.; Baretzky, B.; Goll, D.; Schütz, G. Fe–C nanograined alloys obtained by high pressure torsion: Structure and magnetic properties. *Mater. Sci. Eng. A* **2009**, *503*, 185–189. [CrossRef]
38. Sagaradze, V.V.; Shabashov, V.A. Deformation-induced anomalous phase transformations in nanocrystalline FCC Fe–Ni based alloys. *Nanostruct. Mater.* **1997**, *9*, 681–684. [CrossRef]
39. Ohsaki, S.; Kato, S.; Tsuji, N.; Ohkubo, T.; Hono, K. Bulk mechanical alloying of Cu–Ag and Cu/Zr two-phase microstructures by accumulative roll-bonding process. *Acta Mater.* **2007**, *55*, 2885–2895. [CrossRef]
40. Straumal, B.B.; Dobatkin, S.V.; Rodin, A.O.; Protasova, S.G.; Mazilkin, A.A.; Goll, D.; Baretzky, B. Structure and properties of nanograined Fe–C alloys after severe plastic deformation. *Adv. Eng. Mater.* **2011**, *13*, 463–469. [CrossRef]
41. Sergueeva, A.V.; Song, C.; Valiev, R.Z.; Mukherjee, A.K. Structure and properties of amorphous and nanocrystalline NiTi prepared by severe plastic deformation and annealing. *Mater. Sci. Eng. A* **2003**, *339*, 159–165. [CrossRef]
42. Prokoshkin, S.D.; Khmelevskaya, I.Y.; Dobatkin, S.V.; Trubitsyna, I.B.; Tatyanin, E.V.; Stolyarov, V.V.; Prokofiev, E.A. Alloy composition, deformation temperature, pressure and post-deformation annealing effects in severely deformed Ti-Ni based shape memory alloys. *Acta Mater.* **2005**, *53*, 2703–2714. [CrossRef]
43. Sauvage, X.; Renaud, L.; Deconihout, B.; Blavette, D.; Ping, D.H.; Hono, K. Solid state amorphization in cold drawn Cu/Nb wires. *Acta Mater.* **2001**, *49*, 389–394. [CrossRef]
44. Miyazaki, T.; Terada, D.; Miyajima, Y.; Suryanarayana, C.; Murao, R.; Yokoyama, Y.; Sugiyama, K.; Umemoto, M.; Todaka, T.; Tsuji, N. Synthesis of non-equilibrium phases in immiscible metals mechanically mixed by high pressure torsion. *J. Mater. Sci.* **2011**, *46*, 4296–4301. [CrossRef]

45. Mazilkin, A.A.; Abrosimova, G.E.; Protasova, S.G.; Straumal, B.B.; Schütz, G.; Dobatkin, S.V.; Bakai, A.S. Transmission electron microscopy investigation of boundaries between amorphous "grains" in $Ni_{50}Nb_{20}Y_{30}$ alloy. *J. Mater. Sci.* **2011**, *46*, 4336–4342. [CrossRef]
46. Straumal, B.B.; Mazilkin, A.A.; Protasova, S.G.; Goll, D.; Baretzky, B.; Bakai, A.S.; Dobatkin, S.V. Formation of two amorphous phases in the $Ni_{60}Nb_{18}Y_{22}$ alloy after high pressure torsion. *Kovove Mater.–Metall. Mater.* **2011**, *49*, 17–22. [CrossRef]
47. Straumal, B.B.; Kilmametov, A.R.; Ivanisenko, Y.; Mazilkin, A.A.; Kogtenkova, O.A.; Kurmanaeva, L.; Korneva, A.; Zięba, P.; Baretzky, B. Phase transitions induced by severe plastic deformation: Steady-state and equifinality. *Int. J. Mater. Res.* **2015**, *106*, 657–664. [CrossRef]
48. Straumal, B.B.; Kilmametov, A.R.; Ivanisenko, Y.; Gornakova, A.S.; Mazilkin, A.A.; Kriegel, M.J.; Fabrichnaya, O.B.; Baretzky, B.; Hahn, H. Phase transformations in Ti-Fe alloys induced by high pressure torsion. *Adv. Eng. Mater.* **2015**, *17*, 1835–1841. [CrossRef]
49. Gornakova, A.S.; Straumal, A.B.; Khodos, I.I.; Gnesin, I.B.; Mazilkin, A.A.; Afonikova, N.S.; Straumal, B.B. Effect of composition, annealing temperature and high pressure torsion on structure and hardness of Ti–V and Ti–V–Al alloys. *J. Appl. Phys.* **2019**, *125*, 082522. [CrossRef]
50. Straumal, B.B.; Pontikis, V.; Kilmametov, A.R.; Mazilkin, A.A.; Dobatkin, S.V.; Baretzky, B. Competition between precipitation and dissolution in Cu–Ag alloys under high pressure torsion. *Acta Mater.* **2017**, *122*, 60–71. [CrossRef]
51. Zaher, G.; Lomakin, I.; Enikeev, N.; Jouen, S.; Saiter-Fourcin, A.; Sauvage, X. Influence of strain rate and Sn in solid solution on the grain refinement and crystalline defect density in severely deformed Cu. *Mater. Today Commun.* **2021**, *26*, 101746. [CrossRef]
52. Huang, C.X.; Yang, G.; Gao, Y.L.; Wu, S.D.; Li, S.X. Investigation on the nucleation mechanism of deformation-induced martensite in an austenitic stainless steel under severe plastic deformation. *J. Mater. Res.* **2007**, *22*, 724–729. [CrossRef]
53. Waitz, T.; Pranger, W.; Antretter, T.; Fischer, F.D.; Karnthaler, H.P. Competing accommodation mechanisms of the martensite in nanocrystalline NiTi shape memory alloys. *Mater. Sci. Eng. A* **2008**, *481–482*, 479–483. [CrossRef]
54. Jiang, S.; Zhang, Y.; Zhao, L.; Zheng, Y. Influence of annealing on NiTi shape memory alloy subjected to severe plastic deformation. *Intermetallics* **2013**, *32*, 344–351. [CrossRef]
55. Ivanisenko, Y.; Kilmametov, A.; Roesner, H.; Valiev, R.Z. Evidence of $\alpha \rightarrow \omega$ phase transition in titanium after high pressure torsion. *Int. J. Mater. Res.* **2008**, *99*, 36–41. [CrossRef]
56. Straumal, B.B.; Kilmametov, A.R.; López, G.A.; López-Ferreño, I.; Nó, M.L.; San Juan, J.; Hahn, H.; Baretzky, B. High-pressure torsion driven phase transformations in Cu–Al–Ni shape memory alloys. *Acta Mater.* **2017**, *125*, 274–285. [CrossRef]
57. Straumal, B.B.; Gornakova, A.S.; Mazilkin, A.A.; Fabrichnaya, O.B.; Kriegel, M.J.; Baretzky, B.; Jiang, J.-Z.; Dobatkin, S.V. Phase transformations in the severely plastically deformed Zr–Nb alloys. *Mater. Lett.* **2012**, *81*, 225–228. [CrossRef]
58. Valiev, R.Z. Nanostructuring of metals by severe plastic deformation for advanced properties. *Nat. Mater.* **2004**, *3*, 511–516. [CrossRef] [PubMed]
59. Valiev, R.Z.; Alexandrov, I.V.; Zhu, Y.T.; Lowe, T.C. Paradox of strength and ductility in metals processed by severe plastic deformation. *J. Mater. Res.* **2002**, *17*, 5–8. [CrossRef]
60. Korneva, A.; Straumal, B.; Kilmametov, A.; Gornakova, A.; Wierzbicka-Miernik, A.; Lityńska-Dobrzyńska, L.; Chulist, R.; Gondek, Ł.; Cios, G.; Zięba, P. Omega phase formation in Ti–3wt.%Nb alloy induced by high-pressure torsion. *Materials* **2021**, *14*, 2262. [CrossRef]
61. Rogachev, S.O.; Nikulin, S.A.; Rozhnov, A.B.; Gorshenkov, M.V. Microstructure, Phase composition, and thermal stability of two zirconium alloys subjected to high-pressure torsion at different temperatures. *Adv. Eng. Mater.* **2018**, *20*, 1800151. [CrossRef]
62. Kao, Y.L.; Tu, G.C.; Huang, C.A.; Liu, T.T. A study on the hardness variation of α- and β-pure titanium with different grain sizes. *Mater. Sci. Eng. A* **2005**, *398*, 93–98. [CrossRef]
63. Kilmametov, A.; Ivanisenko, Y.; Mazilkin, A.; Straumal, B.; Gornakova, A.; Fabrichnaya, O.; Kriegel, M.; Rafaja, D.; Hahn, H. The $\alpha \rightarrow \omega$ and $\beta \rightarrow \omega$ phase transformations in Ti–Fe alloys under high-pressure torsion. *Acta Mater.* **2018**, *144*, 337–351. [CrossRef]
64. Gupta, S.C.; Joshi, K.D.; Banerjee, S. Experimental and theoretical investigations on *d* and *f* electron systems under high pressure. *Metall. Mater. Trans. A* **2008**, *39*, 1593–1601. [CrossRef]
65. Hennig, R.; Trinkle, D.R.; Bouchet, J.; Srinivasan, S.G.; Albers, R.C.; Wilkins, J.W. Impurities block the alpha to omega martensitic transformation in titanium. *Nat. Mater.* **2005**, *4*, 129–133. [CrossRef]
66. Afonikova, N.S.; Degtyareva, V.F.; Litvin, Y.A.; Rabinkin, A.G.; Skakov, Y.A. Superconductivity and crystal structure of Ti-Nb alloys after high-pressure action up 120 kbar. *Sov. Phys. Sol. State* **1973**, *15*, 746–749.
67. Vohra, Y.K.; Sikka, S.K.; Menon, E.S.K.; Krishnan, R. High-pressure studies on a prototype omega forming alloy system. *Acta Metall.* **1981**, *29*, 457–470. [CrossRef]
68. Dey, G.K.; Tewari, R.; Banerjee, S.; Jyoti, G.; Gupta, S.C.; Joshi, K.D.; Sikka, S.K. Formation of a shock deformation induced omega phase in Zr20Nb alloy. *Acta Mater.* **2004**, *52*, 5243–5254. [CrossRef]
69. Gornakova, A.S.; Straumal, B.B.; Golovin, Y.I.; Afonikova, N.S.; Pirozhkova, T.S.; Tyurin, A.I. Phase transformations and mechanical properties of two-component titanium alloys after heat treatment in the two-phase region (α + TiMe) and HPT. *J. Surf. Investig. X-Ray Synch. Neutron Tech.* **2021**, *11*, 1–6. [CrossRef]
70. Golovin, Y.I. Nanoindentation and mechanical properties of materials at submicro- and nanoscale levels: Recent results and achievements. *Phys. Solid State* **2021**, *63*, 1–41. [CrossRef]

71. Golovin, Y.I.; Tyurin, A.I.; Aslanyan, E.G.; Pirozhkova, T.S.; Vasyukov, V.M. The physical and mechanical properties and local deformation micromechanisms in materials with different dependence of hardness on the depth of print. *Phys. Solid State* **2017**, *59*, 1803–1811. [CrossRef]
72. Golovin, Y.I.; Tyurin, A.I.; Iunin, Y.L. Strain-rate sensitivity of the hardness of crystalline materials under dynamic nanoindentation. *Dokl. Phys.* **2003**, *48*, 505–511. [CrossRef]
73. Chong, Y.; Zheng, R.; Deng, G.; Shibata, A.; Tsuji, N. Investigation on the microstructure and mechanical properties of Ti–1.0Fe alloy with equiaxed α + β microstructures. *Metall. Mater. Trans. A* **2020**, *51A*, 2851–2863. [CrossRef]
74. Chong, Y.; Deng, G.; Shibata, A.; Tsuji, N. Microstructure evolution and phase transformation of Ti–1.0 wt%Fe alloy with an equiaxed α + β initial microstructure during high-pressure torsion and subsequent annealing. *Adv. Eng. Mater.* **2019**, *21*, 1900607. [CrossRef]
75. Verestiuc, L.; Spataru, M.-C.; Baltatu, M.S.; Butnaru, M.; Solcan, C.; Sandu, A.V.; Voiculescu, I.; Geanta, V.; Vizureanu, P. New Ti–Mo–Si materials for bone prosthesis applications. *J. Mech. Behav. Biomed. Mater.* **2021**, *113*, 104198. [CrossRef] [PubMed]
76. Tane, M.; Okuda, Y.; Todaka, Y.; Ogi, H.; Nagakubo, A. Elastic properties of single-crystalline x phase in titanium. *Acta Mater.* **2013**, *61*, 7543–7554. [CrossRef]
77. Straumal, B.B.; Korneva, A.; Kilmametov, A.R.; Lityńska-Dobrzyńska, L.; Gornakova, A.S.; Chulist, R.; Karpov, M.I.; Zięba, P. Structural and mechanical properties of Ti–Co alloys treated by high pressure torsion. *Materials* **2019**, *12*, 426. [CrossRef] [PubMed]